Evidence of pore correlation in porous silicon: An x-ray grazing-incidence study

V. Chamard,[1,*] P. Bastie,[1] D. Le Bolloch,[2] G. Dolino,[1] E. Elkaïm,[3] C. Ferrero,[2] J.-P. Lauriat,[3] F. Rieutord,[4] and D. Thiaudière[3]

[1]*Laboratoire de Spectrométrie Physique, Université J. Fourier Grenoble 1 - CNRS UMR 5588, BP 87, 38402 Saint Martin d'Hères Cedex, France*

[2]*European Synchrotron Radiation Facility, BP 220, 38043 Grenoble Cedex, France*

[3]*Laboratoire pour l'Utilisation du Rayonnement Electromagnétique, Orsay, France*

[4]*Commissariat à l'Énergie Atomique, Département de Recherche Fondamentale sur la Matière Condensée, CEA/Grenoble, 17 rue des Martyrs, 38054 Grenoble Cedex 9, France*

(Received 11 July 2001; revised manuscript received 25 September 2001; published 4 December 2001)

The structure of porous silicon is investigated by grazing incidence x-ray scattering. Using GISAXS (grazing incidence small-angle x-ray scattering), a systematic pore correlation is observed for all porous silicon types. The quantitative analysis of the measurement has been performed for the p^--type sample, using a spherical model of pores and an isotropic distribution of scattering particles, leading to a typical pore size of 6.2 nm and to a particle-particle correlation length of 8.6 nm. In addition for this type of porous silicon, the morphology of the surface and interface of the layer have been studied by specular and off-specular reflectivity. The roughening due to the pore front propagation is quantified and the interface instability of p^--type porous silicon is observed.

DOI: 10.1103/PhysRevB.64.245416 PACS number(s): 61.10.Eq, 61.10.Kw, 68.55.Ac, 68.35.Ct

Since 1990, the discovery of the room-temperature luminescence of porous silicon (PS) has stimulated much research.[1] However, in spite of the existence of many theoretical models for PS formation, based either on electrochemical or physical properties of semiconductors,[2] the formation mechanisms of this nanocrystalline material are still unclear due to the difficulty of characterizing very thin porous layers. Direct and local characterization is obtained by transmission electron microscopy (TEM). For p^--type PS, the pores are rather isotropic, with diameter around 3 nm, while in p^+-type, larger dendritic pores with a diameter around 8 nm are connected to smaller branching pores with a diameter around 4 nm.[3] The case of n-type PS is more complex due to the large variety of observed morphologies.[4] Some additional information obtained in a nondestructive way and averaged over a large amount of PS material can be obtained by x-ray diffuse scattering measurement either around the transmitted beam [small-angle x-ray scattering (SAXS)] (Ref. 5) or around the Bragg peak of the PS single crystal layer [wide-angle x-ray scattering (WAXS)] (Ref. 6) even using grazing incidence diffraction (GID).[7,8] The most important results are the clear anisotropy of p^+-type PS pores and the presence of a strong particle-particle correlation in this material. Some results on n-type PS have been also reported.[5,7]

PS is obtained by the anodization of a silicon single crystal in an electrolytic solution containing hydrofluoric acid (HF), ethanol, and water. Layers with a thickness from a few tens to thousands nanometers can be prepared by adjusting the formation time. In this thickness range, x-ray scattering techniques in grazing incidence geometry are well adapted measurements for the determination of the PS structure. The combination of measurements performed in the plane[7,9–12] and out of the plane of incidence results in information with length scales ranging from a few to hundreds of nanometers.

In this paper, we present a structural investigation of different types of PS samples. After a brief description of the experimental conditions, we first report on the observation on systematic correlations in various PS layers using out-of-plane GISAXS (grazing incidence small-angle x-ray scattering).[13] This technique is rather sensitive to the bulk scattering from the particles in the near surface region. For the p^--type sample, a quantitative analysis of pore size and correlation length has been performed. We complete the structural investigation of p^--type PS by the characterization of both external surface and interface of the PS layer using in-plane measurements, i.e., specular and off-specular reflectivity.

For x rays, the real part of the index of refraction is a little smaller than unity and leads to the existence of a total external reflection regime for incident angle α_i smaller than a critical angle α_c.[14] The value of α_c, in the order of a few tenths of a degree, depends on the electron density near the surface. For porous silicon, α_c is directly related to the porosity P of the layer,[7]

$$P=1-\left(\frac{\alpha_{\mathrm{c,PS}}}{\alpha_{\mathrm{c,Si}}}\right)^2, \tag{1}$$

where $\alpha_{\mathrm{c,PS}}$ and $\alpha_{\mathrm{c,Si}}$ are the critical angles of the porous silicon layer and silicon substrate, respectively. The specular reflectivity (measured for $\alpha_i=\alpha_f$, where α_f is the exit angle) is sensitive to the electron density profile along the q_z axis, normal to the sample surface.[14] Additional scattered intensity results, in both specular and off-specular directions, from defects at the interfaces (roughness) or in bulk (pores and particles). We report on two kinds of experiments. For an in-plane geometry measurement, i.e., $2\theta=0$ [see scheme in Fig. 1(a)], the information obtained along q_z concern the small length scale structure (in the range of a few nanometers), while in the lateral direction along q_x, larger length

 ©2001 The American Physical Society

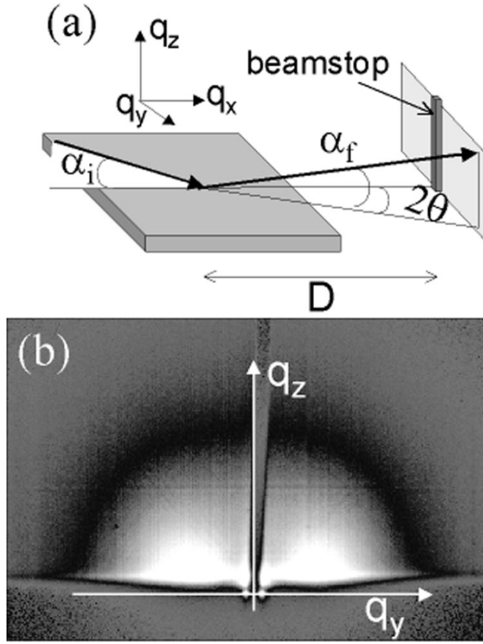

FIG. 1. (a) Scheme of the scattering geometries used for in-plane specular and off-specular measurements ($2\theta=0$) and for out-of-plane GISAXS ($2\theta\neq 0$). (b) GISAXS pattern measured on sample p_1^-.

scale is probed (a few tens of nanometers). The reflected intensity is most sensitive to the surface and interface structure and the PS layer can be considered as a homogeneous medium. The analysis of specular and off-specular intensities are performed using routines developed and tested by Tolan and Press:[14] the Parrat formalism is used for the specular part, while the analysis of the diffuse scattered intensity is obtained within the distorted-wave Born approximation (DWBA), which assumes self-affine roughness structure of interfaces. The height-height correlation function $C(R)$ introduced by Sinha *et al.*[15] for fractal interfaces in the Gaussian approximation is given by

$$C(\mathbf{r})=\sigma^2\exp[-(\mathbf{r}/\xi_{\parallel})^{2h}], \tag{2}$$

where $\mathbf{r}$ is the lateral position vector, scanning the interface, $\xi_{\parallel}$ is the lateral cutoff length, h is the Hurst parameter, and σ is the root-mean-square roughness: this last parameter is given by the full width at half maximum of the derivative of the electron density profile at the interface. These measurements have been performed using synchrotron radiation at LURE, on WDIF4C beamline, with a wavelength λ of 0.128 nm. A crystal analyzer has been used to increase the resolution.

In the GISAXS geometry, where the out-of-plane signal is measured ($2\theta\neq 0$),[13] the scattered intensity in the (q_y,q_z) plane is sensitive to defects in the nanometer range,[16] corresponding to the pore/crystallite typical size. Generally in GISAXS, the intensity is described by

$$I(q)=T(\alpha_i^*)S(q)C(q)T(\alpha_f^*), \tag{3}$$

TABLE I. Anodization conditions used for fabrication of the five samples investigated: HF concentration of the electrolyte [HF], constant current density *j*, formation time t_f, and thickness *T* of the resulting nanoporous layers.

	Resistivity Ω cm	[HF] (%)	j mA cm^{-2}	t_f s	Light	T nm
p_1^-	5	25	15	160	no	2000
p_2^-	5	17.5	16	3.8	no	40
p^+	10^{-2}	25	10	128	no	2000
n^+	$5\ 10^{-3}$	15	5	400	no	2000
n^-	5	15	5	300	yes	1000

where $T(\alpha_{i,f}^*)$ is the transmission factor for the incidence and exit angles in the medium, $S(q)$ is the shape factor of a single particle, and $C(q)$ is the particle-particle correlation term. The choice of $S(q)$ and $C(q)$ for porous silicon will be explained further. The out-of-plane measurements have been obtained on the ID01 beamline at ESRF ($\lambda=0.154$ nm) using a two-dimensional (2D) gas filled detector whose distance D to the sample can be adjusted between 632 and 4032 mm to improve the resolution [Fig. 1(a)].

Five samples, named p_1^-, p_2^-, n^-, n^+, and p^+, have been investigated. They are obtained by the electrochemical anodization of a single-crystal silicon wafer [(001) oriented] in a solution containing HF, ethanol, and water and using a constant current density *j*.[1] The formation conditions of the samples are reported in Table I.[17] The thickness *T* of the PS layers is adjusted by controlling the formation time t_f, which varies from a few seconds to a few hundreds of seconds. The *p*-type substrates are boron doped while *n*-type ones are phosphorus doped. For low doped n^--type, the lack of mobile carriers in silicon is compensated by an illumination during anodization that creates the holes necessary for the electrochemical reaction. The illumination is performed with a halogen lamp and a filter transmitting a power density of 40 mW cm^{-2} for wavelengths larger than 660 nm. After anodization, the samples are rinsed for 5 min in deionized water and dried with N_2 gas.

GISAXS investigation has been performed on samples with thick PS layers in the micrometer range. Then, the intensity mostly results from bulk scattering and the surface scattering can be neglected (the PS/Si interface does not scatter, due to the absorption of the grazing x-ray beam in the PS layer). Figure 1(b) presents the GISAXS pattern obtained for the p^--type sample using $D=1732$ mm and $\alpha_i=0.12°$. For this sample, $\alpha_{c,PS}$ has been measured at 0.16°. The scattered intensity is recorded in the upper range of the detector due to the shadowing effect from the sample surface. A vertical beam stop is used to avoid the strong intensity from the direct and specular beams. Along the q_y axis two intense maxima are observed resulting from a strong anisotropic particle-particle correlation enhanced by the transmission factor at the $\alpha_{c,PS}$ position. At larger q_y a broad diffuse scattered intensity is observed, resulting from the size and shape of the pores. The same kind of experiment has been performed on all the typical kinds of PS samples. Figure 2(a) presents the q_y cross section taken from the GISAXS pattern

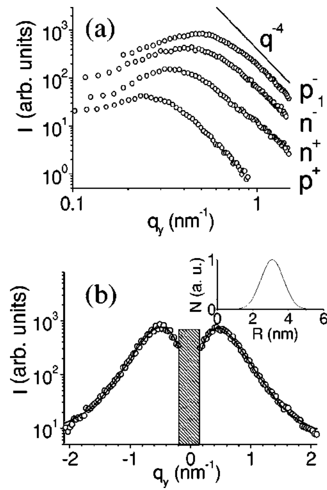

FIG. 2. (a) GISAXS cross sections along the q_y axis for various PS samples (circles) and asymptotic q_y^{-4} decrease (line) represented on a log-log scale. For clarity, the curves have been vertically shifted by an arbitrary factor. (b) GISAXS cross section along q_y measured on sample p_1^- (circles) and result of the best fit using a model with spherical pore isotropically distributed (line); the corresponding radius distribution is shown in the inset.

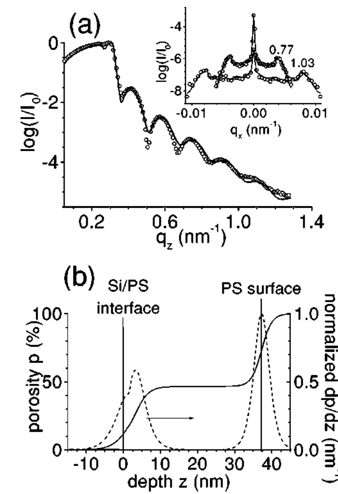

FIG. 3. (a) Specular reflectivity measured on sample p_2^- (circle) and off-specular rocking scan measurements performed at the two q_z values indicated on the graph (inset). The result of the best fit is also presented (line). (b) Resulting porosity profile as a function of depth (continuous line) and its derivative (dashed line).

measured for p_1^-, n^-, n^+, and p^+ samples. They all exhibit a strong correlation maximum and an asymptotic decrease close to the typical q_y^{-4}, following the classical Porod law for sharp interfaces.[18] The correlation maxima of different types of PS are obtained between the small value of p^+-type ($q_y = 0.25\ \mathrm{nm}^{-1}$) and the large value of p^--type ($q_y = 0.5\ \mathrm{nm}^{-1}$). It allows us to compare the typical structural size between all PS types; from the smallest to the largest structure, the following classification is obtained: p^+, n^+, n^-, p^-. In the following, we emphasize the behavior of the p^--type sample. The simulation assumes a spherical shape of the pores with an isotropic distribution of particles in the (q_x, q_y) plane.[19] The spherical pore shape is a rather reasonable estimation, justified by various TEM observations[3] and by the q_y^{-4} decrease.[18] A Gaussian size distribution has been used to take into account the variation in pore size in such a porous medium.[3] Along q_y, $T(\alpha_{i,f}^*)$ remains constant. The result of the best fit is presented in Fig. 2(b). The corresponding numerical values are a pore diameter of 6 nm and a lateral correlation length of 8.6 ± 0.6 nm. The size distribution, presented on the inset of Fig. 2(b), shows a typical size deviation of ± 1.6 nm. However, the model of correlated spheres is very rough and cannot give a true picture of the complex morphology of PS pores: the etched volumes must be interconnected and in communication with the external HF solution. Using the measured parameters for an isotropic distribution of spheres, we find a porosity around 20%, while the determination from the value of the critical reflection angle is 47%. Moreover, the hypothesis of an isotropic structure is clearly inadequate as no correlation is observed along the z axis. In fact, the correlation length, observed in the surface plane, corresponds probably to the average distance between irregular etched channels. The larger value of the porosity can be due to the numerous and irregular branching of dead-end pores. One notes that this is somewhat similar to the pictures of the p^+-type PS structure observed by electron microscopy,[3] but with a smaller size for p^--type samples.

We focus now on the structural characterization of the surface and interface of the p^--type PS layer. For this study, a thin PS layer is chosen to reduce the bulk scattering from pores and particles. Figure 3(a) shows the specular reflectivity curve obtained for sample p_2^-. The critical angle of the porous layer is visible at $q_z = 0.25\ \mathrm{nm}^{-1}$ ($\alpha_{\mathrm{c,PS}} = 0.155°$) and the strong decrease of intensity at $q_z = 0.31\ \mathrm{nm}^{-1}$ ($\alpha_{\mathrm{c,Si}} = 0.185°$ for the chosen λ) corresponds to the bulk silicon substrate one. At larger angles, interference fringes indicate rather sharp interface and surface of the layer. In the inset of Fig. 3(a), two rocking scans are presented. They exhibit strong Yoneda maxima at q_x corresponding to $\alpha_{i,f} = \alpha_{\mathrm{c,PS}}$, that result from the scattering by the roughness of both surface and interface. After some preliminary tests, it has been concluded that a single layer model with the usual symmetric electron density profile[15] was not sufficient to fit these measurements. It is necessary to use an asymmetric profile at the PS/Si interface to describe the porosity variation. This was obtained by introducing, at this interface, a transition layer with a fixed 3-nm thickness. This additional layer leads to the use of four new fitting parameters (P, σ, $\xi_\parallel$, and h); some of them, $\xi_\parallel$ and h, were not free but set to the value of the ones of the PS/Si interface, in order to obtain a satisfying fit with the smallest number of fitting parameters. Although the values of the roughness at both sides of the transition layer were comparable to the layer thickness, a continuous electron density profile was calculated by the program, using the overlapping of the two Gaussian curves in the derivative of the electron density. This allowed us to use a standard program to produce asymmetric profile at the PS/Si interface.[20] This model has been successfully tested on numerous PS samples.[17] Finally, the use of ten free parameters is sufficient for the fit of the three curves of Fig. 3(a),

TABLE II. Values of parameters used for the fit of the specular and off-specular reflectivity [Fig. 3(a)] measured on the thin sample p_2^-. The number in brackets are not free parameters but constrained to the value of the PS/Si interface parameters.

	PS layer	Transition layer	PS/Si interface
P (%)	45±2	15±10	
T (nm)	34.2±0.5	(3)	
σ (nm)	2.2±0.5	2.5±0.5	3.6±0.1
$\xi_\parallel$ (nm)	30±20	(150)	150±100
h	0.15±0.05	(0.15)	0.15±0.05

simultaneously. The resulting values are reported in Table II. Figure 3(b) shows the corresponding porosity profile deduced from the electron density profile. The total thickness of 37.2 nm and the porosity of 46% are directly determined by $\alpha_{c,PS}$ and by the thickness fringes from the specular reflectivity profile. The derivative porosity profile, also plotted in Fig. 3(b), shows the larger roughness of the PS/Si interface (7.5 nm) than of the surface (4.7 nm) resulting from the pores propagation front. The values of Table II show in addition that the lateral cutoff length is larger at the interface than at the surface, and is quite large (150 nm) in regard to the values obtained on other PS types. To compare, for n^+-type PS a lateral cutoff length of about 40 nm has been obtained.[21] In spite of the large error bar resulting from the lack of structure in these measurements, the lateral cutoff length is large and must be related to the interface instability predicted and observed by Chazalviel *et al.* on low doped *p*-type PS.[2] Finally, the small Hurst parameter value (0.15) is the signature of the complex jagged interfaces of the PS layer.

To conclude, we have presented results on GISAXS experiments performed on PS. Thanks to the technique, which is well suited for the characterization of the PS structure near the surface, we have been able to show systematically the strong pore correlation for a large range of PS types (p^-, p^+, n^+, n^-). For both *n*- and *p*-type PS, the typical structural size of the material increases with the doping level. The simulation performed for p^- type shows that the simple model of spherical pores isotropically distributed is suitable to obtain pores size and correlation length, although the real topology of a porous medium is more complex. Further comparative analysis will be performed on the other PS types. Some specular reflectivity measurements on PS have previously been performed,[7,9–12] but without investigation of the off-specular scattered intensity. However, the scattered intensity along q_x contains relevant structural information needed for the knowledge of the height-height correlation function.[21] During our investigation of p^--type, we observed the asymmetric profile of the porosity at the PS/Si interface. The quantitative analysis shows the larger roughness at the interface resulting from the pore front propagation and the large cutoff length of the roughness, that must result from the interface instability.[2] These two techniques will be applied to study the structural changes during growth in the porous structure and at the interface.

Furthermore, the combination of GISAXS and specular and off-specular reflectivity could lead to new results for the investigation of porous materials such as porous semiconductors[1] and other porous layers, where both the interfaces of the layer and of the bulk material present a strong electron density modulation resulting from various fabrication processes.

The authors would like to thank J. Stettner for his help during the analysis of the reflectivity data and M. Tolan and T. H. Metzger for fruitful discussions. We are very grateful to all the technical staff of LURE and ESRF.

*Corresponding author: chamard@esrf.fr; Present address: European Synchrotron Radiation Facility, BP 220, 38043 Grenoble Cedex, France.

[1] A.G. Cullis, L.T. Canham, and P.D. Calcott, J. Appl. Phys. **82**, 909 (1997).
[2] J.-N. Chazalviel, R.B. Wehrspohn, and F. Ozanam, Mater. Sci. Eng., B **69**, 1 (2000).
[3] M.I.J. Beale *et al.*, Appl. Phys. Lett. **46**, 86 (1985).
[4] C. Lévy-Clément, A. Lagoubi, and M. Tomkiewicz, J. Electrochem. Soc. **141**, 958 (1994).
[5] P. Goudeau, A. Naudon, G. Bomchil, and R. Hérino, J. Appl. Phys. **66**, 625 (1989).
[6] D. Buttard, D. Bellet, and G. Dolino, J. Appl. Phys. **79**, 8060 (1996).
[7] A. Bensaid *et al.*, Solid State Commun. **79**, 923 (1991).
[8] M. Binder, T. Edelmann, T.H. Metzger, and J. Peisl, Solid State Commun. **100**, 13 (1996).
[9] E. Chason *et al.*, in *Microcrystalline and Nonocrystalline Semiconductors*, edited by L. Brus, M. Hirose, R. W. Collins, F. Koch, and C. C. Tsai, Mater. Res. Soc. Symp. Proc. **358** (Materials Research Society, Pittsburgh, 1995), p. 321.
[10] J.M. López-Villegas *et al.*, Thin Solid Films **276**, 238 (1996).
[11] D. Buttard *et al.*, Solid State Commun. **109**, 1 (1999).
[12] M. Servidori *et al.*, Solid State Commun. **118**, 85 (2001).
[13] J.R. Levine, J.B. Cohen, Y.W. Chung, and P. Georgopoulos, J. Appl. Crystallogr. **22**, 528 (1989).
[14] M. Tolan and W. Press, Z. Kristallogr. **213**, 319 (1998).
[15] S.K. Sinha, E.B. Sirota, S. Garoff, and H.B. Stanley, Phys. Rev. B **38**, 38 (1988).
[16] A. Guinier and G. Fournet, *Small Angle Scattering of X-rays* (Wiley, New York, 1955).
[17] V. Chamard, Ph.D. thesis, Université Joseph Fourier–Grenoble 1, 2000.
[18] G. Porod, Kolloid-Z. **124**, 83 (1951).
[19] A.F. Bonfiglioli and A. Guinier, Acta Metall. **14**, 1213 (1966).
[20] W. Press, J.-P. Schlomka, M. Tolan, and B. Asmussen, J. Appl. Crystallogr. **30**, 963 (1998).
[21] V. Chamard, G. Dolino, and J. Stettner, Physica B **283**, 135 (2000).